

Finite Element Shape Optimization for Biodegradable Magnesium Alloy Stents

W. WU,¹ L. PETRINI,¹ D. GASTALDI,¹ T. VILLA,¹ M. VEDANI,² E. LESMA,² B. PREVITALI,²
and F. MIGLIAVACCA¹

¹Laboratory of Biological Structure Mechanics, Department of Structural Engineering, Politecnico di Milano, Piazza Leonardo da Vinci, 32, 20133 Milan, Italy; and ²Department of Mechanical Engineering, Politecnico di Milano, Milan, Italy

(Received 19 January 2010; accepted 23 April 2010; published online 6 May 2010)

Associate Editor Jane Grande-Allen oversaw the review of this article.

Abstract—Biodegradable magnesium alloy stents (MAS) are a promising solution for long-term adverse events caused by interactions between vessels and permanent stent platforms of drug eluting stents. However, the existing MAS showed severe lumen loss after a few months: too short degradation time may be the main reason for this drawback. In this study, a new design concept of MAS was proposed and a shape optimization method with finite element analysis was applied on two-dimensional (2D) stent models considering four different magnesium alloys: AZ80, AZ31, ZM21, and WE43. A morphing procedure was utilized to facilitate the optimization. Two experiments were carried out for a preliminary validation of the 2D models with good results. The optimized designs were compared to an existing MAS by means of three-dimensional finite element analysis. The results showed that the final optimized design with alloy WE43, compared to the existing MAS, has an increased strut width by approximately 48%, improved safety properties (decreased the maximum principal stress after recoil with tissue by 29%, and decreased the maximum principal strain during expansion by 14%) and improved scaffolding ability (increased by 24%). Accordingly, the degradation time can be expected to extend. The used methodology provides a convenient and practical way to develop novel MAS designs.

Keywords—Minimally invasive device, Computational analysis, Optimized design, Bioabsorbable device, Experimental tests.

INTRODUCTION

Biological incompatibility between vessels and permanent coronary stent platforms (usually of stainless steel, SS) may have long-term adverse effects, though

drug eluting stents have reduced in-stent restenosis effectively.²⁴ Biodegradable magnesium alloy stents (MAS) provide a temporary scaffolding to target vessels, degrade gradually and are ultimately absorbed by the body.²⁵ The Magic stent (Biotronic Inc., Germany) of magnesium alloy WE43 is the only existing MAS that has gone through animal and clinical trials, showing safety and similar scaffolding properties as SS stents just after implantation.^{16,21,26} However, a multicenter trial of the Magic stent showed that after four months of implantation, the vessel lumen loss was severe.⁵ The main reason for this drawback may be that the Magic stent degrades too fast, and the period to resist corrosion (i.e., to maintain structural integrity) is not sufficient.²² Besides the development of enhanced materials to extend corrosion time,⁷ new stent designs from shape optimization can be one option to increase corrosion resistance and to improve mechanical properties, simultaneously.

Since the tiny stent structure and the high cost of prototype make *in vitro* testing difficult, finite element analysis (FEA) has become a typical research tool to test stent properties in the following different conditions: expansion,^{6,9} flexibility,^{14,19} fatigue,^{12,17} and interaction with tissues.^{1,10,18} However, only a few shape optimization works based on FEA have been performed up to now.^{11,23} According to Li *et al.*,¹¹ shape optimization of stents is a difficult task in the following respects: (i) a series of parameterized geometric models are required, which implies lots of repeated modeling and meshing procedures; (ii) optimization loops and transporting of the parametric models among different software may have to be hindered by manual interactions; and (iii) convergence failure should be avoided as possible. Furthermore, a MAS has two controversial requirements in mechanical

Address correspondence to L. Petrini, Laboratory of Biological Structure Mechanics, Department of Structural Engineering, Politecnico di Milano, Piazza Leonardo da Vinci, 32, 20133 Milan, Italy. Electronic mail: lorenza.petrini@polimi.it

properties compared to a conventional SS stent. First, SS stents undergo a large local strain (about 0.4–0.5) during stent expansion,¹³ while most magnesium alloys have a much lower ultimate elongation (usually below 0.2)²; therefore, the excessive strain of a MAS during expansion needs to be avoided. Second, the elastic modulus of magnesium alloys is about 25% of SS, thus a MAS needs more material (e.g., widening stent strut) to provide adequate scaffolding. However, more material may increase the strain during expansion. Moreover, the degradation time, which is mainly controlled by both uniform and stress corrosion processes,²⁸ requires at the same time an increase in mass and a reduction in maximum stress during scaffolding.

In this study, a shape optimization method for MAS was proposed and two-dimensional (2D) stent models of a new design concept were optimized considering four magnesium alloys. A morphing procedure was utilized to facilitate the optimization. Two simple experiments were carried out for the preliminary

validation of the 2D model. The optimized designs were used to create 3D stent structures: their performance was numerically (FEA) compared to the existing MAS inserting the stents inside a stenotic artery model. The objective of this study is to show a shape optimization method for MAS, and to provide an optimized design with increased material and improved mechanical properties and, accordingly, an expected extended degradation time compared to the existing MAS.

MATERIALS AND METHODS

Geometry Models

The CAD models of a stent resembling the existing Magic stent (also named as the Magic stent in the paper for simplicity) and of a new conceptive stent are shown in Figs. 1a and 1b, respectively. The Magic stent was taken from literature⁵ and it has seven rings

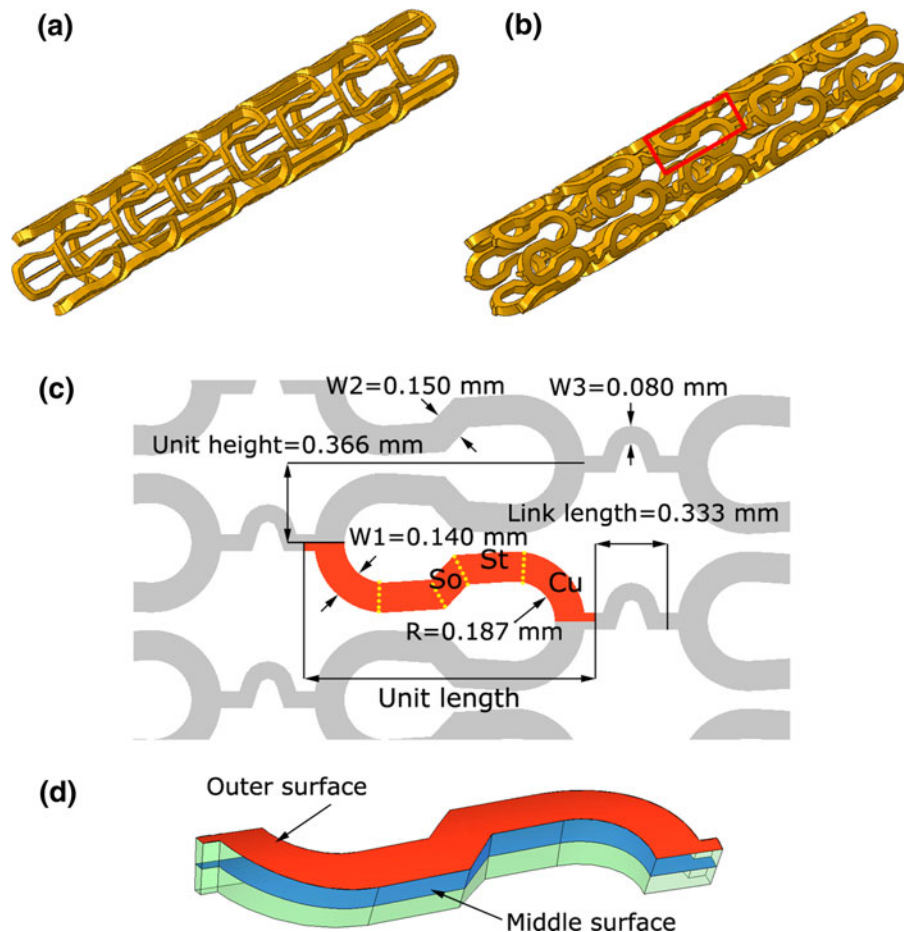


FIGURE 1. (a) The CAD model resembling the Magic stent (Biotronik, Berlin, Germany). (b) The CAD model of the new conceptive stent in the original configuration. One strut unit (in the box) was chosen for the optimization. (c) 2D Dimensions of the new conceptive stent (outer surface). The strut unit for optimization is shaded. The unit is composed of curved (Cu), straight (St), and solidus (So) parts. (d) Illustration of the outer and middle surfaces of the unit. The middle surface was used as the 2D optimization model (M_{2d}) after being projected to a plane.

connected by straight links, presenting four peak-to-valley struts in the circular direction. It was reconstructed with an outer diameter of 1.4 mm, a longitudinal length of 8.0 mm, a thickness of 0.15 mm, and a strut width of 0.08 mm. The new conceptive stent was developed with the help of a classical topology optimization procedure.³⁰ The design has five rings connected by curved links, presenting six peak-to-valley struts in the circular direction. The dimensions of the outer diameter (1.4 mm) and thickness (0.15 mm) were arbitrarily fixed equal to those of the Magic stent. Its dimensional details are shown in Fig. 1c, where the “rolled back” outer surface is depicted. The strut width was increased to 0.14 mm if compared to the Magic stent. Only one strut unit was chosen for optimization for the highly symmetrical design (Figs. 1b and 1c). The unit has two curved (Cu) and two straight (St) parts linked by a solidus (So) part, see Fig. 1c. Considering that a 2D stent model can well represent the corresponding 3D model in expansion,^{4,14} the 2D model (M_{2d}) of the new design was built by extracting the middle surface of the unit and projecting it onto a plane.

Material Properties

Four magnesium alloys were considered: AZ80, AZ31, ZM21, and WE43. Specimens of the first three alloys were available and their mechanical characteristics were measured in a series of tensile testing; while tensile properties of WE43 were taken from literature.¹⁵ All of the alloys have the same modulus (45 GPa), Poisson’s ratio (0.3), and density (1.74 g/mm³). The true strain–true stress curves of these alloys are shown in Fig. 2. Because magnesium alloys are

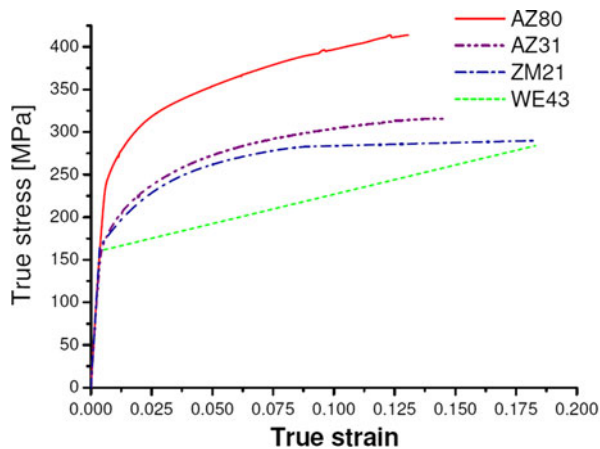


FIGURE 2. True strain–true stress curves of magnesium alloys AZ80, AZ31, ZM21, and WE43. The curves were transformed from experimental testing except the WE43 curve, which was taken from the literature.¹⁵

more brittle than SS, 80% of the ultimate elongation was set as the optimization limit (Opt-limit) for each alloy, which implies that the maximum principal strain during expansion of the optimized design must be below the Opt-limit. Table 1 lists yield stresses, ultimate elongation, and Opt-limits of each alloy investigated.

Meshing, Boundary Conditions, and Loading Steps

The M_{2d} was imported into a parametric CAD software and meshed with 428 shell elements (with the thickness of 0.15 mm), see Fig. 3. The boundary conditions kept the M_{2d} deforming onto the plane. In the first loading step, a vertical displacement of 0.418 mm was applied to the end of the curved part: it was equivalent to expand the 3D stent model to an outer diameter of 3.0 mm. In the second step, the displacement loading was removed and the M_{2d} recoiled freely. A commercial FEA code was used for the simulations. The number of elements was increased by four times to test mesh sensitivity and the results in terms of strain differed less than 2% to each other.

Under the loading conditions, a reduction of the unit length increased the maximum principle strain. If the maximum principle strain increases beyond the ultimate elongation, the stent structure breaks at the strain concentrated locations. Thus, three unit lengths (1.45, 1.36, and 1.22 mm) were set when the maximum principal strains of the M_{2d} with AZ80, AZ31, and WE43 reached their respective ultimate elongation. ZM21 has the same ultimate elongation of WE43 and, for the sake of simplicity, the same unit length was also adopted.

TABLE 1. Tensile properties of magnesium alloys.

	AZ80	AZ31	ZM21	WE43*
Yield stress (MPa)	230	153	165	161
Ultimate tensile strain	0.131	0.146	0.183	0.183
80% of ultimate strain	0.105	0.117	0.146	0.146

*Properties for WE43 were taken from literature.¹⁵

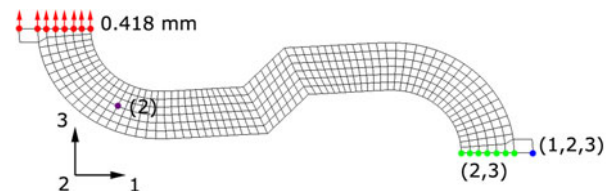


FIGURE 3. Boundary conditions and displacement loadings for the M_{2d} .

Morphing Procedure

The shape of a M_{2d} was changed following a morphing procedure (Fig. 4): a few nodes at the edges of a shape domain (all the elements) were set as handles to control the change of the shape domain. With reference to the original design, the M_{2d} was projected onto the 2D outer surface (Fig. 1b). Four different shapes (shapes 1–4) were set with variations at the ends of the curved parts, the middle curved parts, the middle straight parts, and the sides of the solidus part, respectively. The range of shape changes is the original width ± 0.02 mm for each shape, according to a shape factor changing between 1 and -1 . When the handles moved, the shape of the domain changed, and in turn the positions of the nodes inside the domain changed, see Fig. 4. During this process the mesh morphed with the grid continuity due to continuous shape functions applied to all the nodes of the domain. Each shape variation changed continuously in the range assigned, consequently there could be infinite design possibilities. Furthermore, shape variations were set separately but they influenced each other. For example, when all shapes overlapped with factor -1 , the minimum strut width was 0.105 mm. It implies that compared to the Magic stent, the optimized design

increased the width by 30% at least. After definition of the shape variations, the M_{2d} was projected back to 2D middle surface and the shape variations changed accordingly (e.g., the minimum strut width was 0.094 mm when all shapes overlap with factor -1).

Optimization Procedure and Validation Testing

The optimization flow chart is shown in Fig. 5. An optimization algorithm based on the adaptive response surface method (ARSM)²⁷ was applied to control the shape evolution.

The original 2D model was transferred from the parametric CAD to the FEA code for the initial simulation. Successively, the maximum principal strain, the mass, and the recoil ratio were extracted as initial responses. Because three unit lengths were investigated, the mass was normalized by unit length (norm. mass) for comparison. The recoil ratio was calculated as

$$\text{recoil ratio} = \frac{\text{max. unit height} - \text{unit height after recoil}}{\text{max. unit height}} \times 100. \quad (1)$$

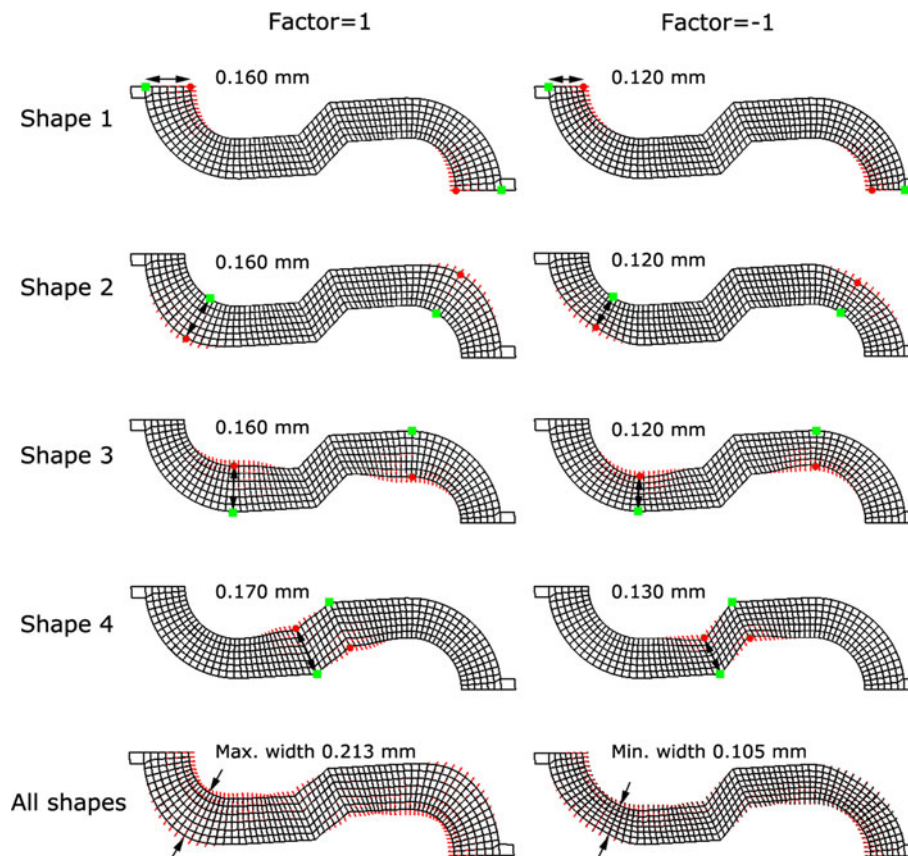


FIGURE 4. Illustrations of shape variations. The moved and fixed handles are indicated as circles and squares, respectively.

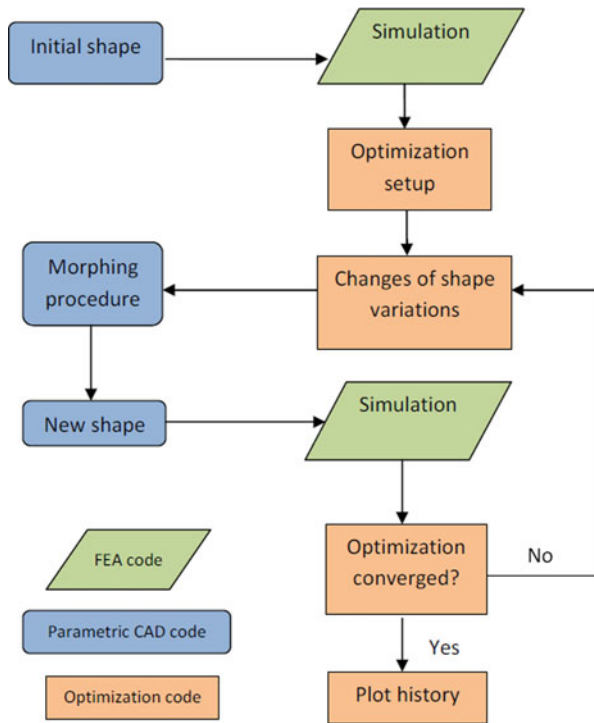


FIGURE 5. Flow chart of the shape optimization procedure for the M_{2d} .

As described in the “Introduction”, the two main optimization objectives (i.e., minimizing maximum principal strain and maximizing mass or strut width) contradict each other. A multi-objective optimization approach can be avoided if a hierarchy between the priority of the objectives is definable. In this study, the highest priority was assigned to the strain limit. In this sense, a two-step strategy was applied to find a proper design comprising the main objectives. The recoil was not involved in the optimization and was set as a reference response.

First, only the maximum strain was minimized. The optimization, performed using a commercial code, was formulated as

$$\text{Minimize } \max. \text{ principal strain} \quad (2)$$

$$\text{Subject to } -1 \leq \text{shape factor} \leq 1 \quad (3)$$

In the first optimization loop, the optimization code changed the shape factor for each shape variation, and the morphing procedure created a new shape. An input file of the new shape was obtained for the FEA code to produce updated responses. Successively, the optimization code recorded the history of responses and verified whether the response of maximum principal strain satisfied the default convergence criterion. The relative change in maximum principal strain over the two last iterations smaller than 0.01 represents the

convergence criterion adopted. If not, a new loop starts and the optimization process continued until the convergence was reached. In the optimization history, each iteration (loop) corresponded to a new shape.

Second, the design with maximum normalized mass was chosen as an optimized design from optimization iterations whose maximum principal strains were below the Opt-limit. For each material, all three unit lengths were analyzed and the best optimized design was chosen to construct the 3D stent model.

For the preliminary model validation, 2D magnesium specimens were manufactured and experimentally tested for recoil and fracture. AZ31 sheets with the thickness of 0.38 ± 0.05 mm were cut by laser according to the original and optimized designs with the unit length of 1.36 mm. The designs were scaled 2.5 times in order to overcome the disadvantages of the low laser accuracy and heat affected zone. A fiber laser (50 W pulsed, 80 kHz pulse frequency) was utilized at a speed of 3 mm/s in conjunction with Argon gas for protection; no electropolishing was carried out. Accordingly, a net of 12 rings composed by 10 struts (20 units) each was produced, being available a cutting area of $50 \text{ mm} \times 16.35 \text{ mm}$. Tensile tests were performed on a MTS 858 MiniBionix testing machine (MTS Systems, Minneapolis, MN, USA) under displacement control at 5 mm/min speed. The specimens for the recoil testing were stretched until each unit had the displacement of 1.045 mm and then released. The recoil ratio was calculated as formulate (1). Each recoil test was repeated three times and the results were averaged. The specimens for the fracture testing were stretched until each specimen structure broke and the displacements were recorded.

3D Model

The FEA model for 3D simulation was composed of a stent, a folded balloon and a vessel including a plaque, see Fig. 6a. The vessel has a longitudinal length of 23 mm, an inner diameter of 3.0 mm and a thickness of 0.5 mm. The plaque has a longitudinal length of 7 mm, an inner diameter of 2.0 mm and a thickness of 0.5 mm. The balloon has a longitudinal length of 10 mm, a folded diameter of 1.05 mm and a dilated diameter of 2.75 mm. The stent, balloon, and tissue are coaxial and the middle points of all axes are superimposed. Figure 6b illustrates the balloon folded in the stent. The balloon was meshed with membrane elements and other components (stent and tissue) with solid elements. The material formulas of balloon and tissue were those adopted by Gervaso *et al.*⁶ A quasi-static procedure of a FEA explicit solver was applied in the simulations. The ends of the vessel were fixed and the balloon ends were constrained in the axial

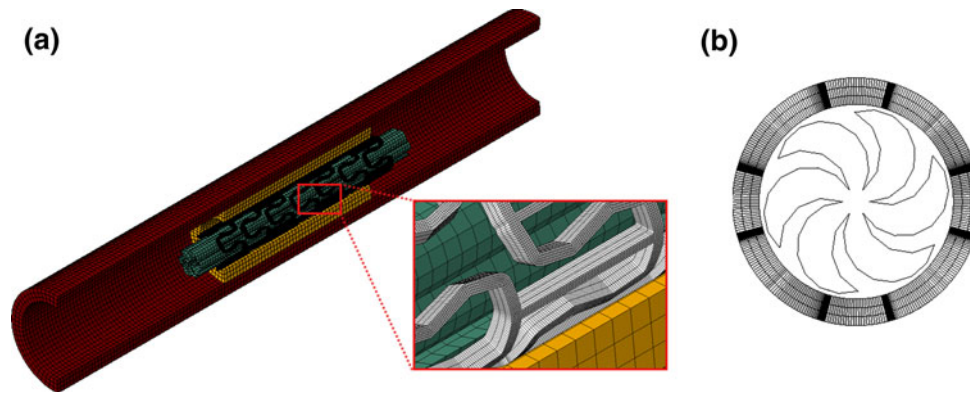


FIGURE 6. (a) Meshes of the 3D model, including the stent, the balloon, and the arterial vessel. (b) The frontal view of the balloon folded inside the stent.

direction. The interactions between the balloon, stent, and plaque had a friction with a factor of 0.2.³ A pressure of 0.6 MPa was imposed on the internal surface of the balloon to expand the stent and tissue. Successively the pressure decreased to zero and the stent recoiled with the scaffolding of the tissue. The maximum principal strain, normalized mass, recoil, and maximum principal stress after stent recoil were analyzed.

RESULTS

2D Optimization Results

The maximum principal strain of the WE43 M_{2d} with the unit length of 1.22 mm generally decreased with reduction of the mass, and the optimization reached convergence after 26 iterations with a maximum principal strain of 0.125 (Fig. 7a). For convenience of observation, iterations with the maximum principal strains below Opt-limit (0.146) were shaded. Iteration 23 had the highest normalized mass ($3.50 \text{ g} \cdot \text{e}^{-5}/\text{mm}$) in the shaded results. Thus the shape of iteration 23 was chosen as the optimized design for this M_{2d} . Figure 7b shows the optimization history of shape variations, and the layout comparison between the original and optimized designs (after projected to the 2D outer surface) is shown in Fig. 7c. It can be observed that the shape variation of the straight strut parts (shape3) contributed the most to the new layout of the optimized design while the variation in the solidus part (shape4) contributed the least. The comparison of maximum principal strain distribution at the end of the loading step between the original and optimized designs is shown in Fig. 8. There was a strain concentration in the inner curved parts of the original design, while the strain of the optimized design was more evenly distributed along the curved parts.

As for the other 2D models, when the unit length was 1.45 mm the original designs of ZM21 and WE43 had the maximum (max.) principal strains below their Opt-limits, which consequently did not need optimization (Table 2). When the unit length was 1.36 mm, the maximum principal strain of the original design with AZ80 was beyond the ultimate elongation, hence the other results were not applicable (N.A.); however, the optimized design of this case was below Opt-limit. When the unit length was 1.22 mm, the maximum principal strains of both the original and optimized design with AZ80 and AZ31 were all beyond the ultimate elongation and Opt-limits, respectively. For ZM21, the maximum principal strain of the original design was beyond the ultimate elongation (which is N.A.), but that of optimized design was below Opt-limit. It can be observed that the recoil decreased when the unit length decreased. The optimization decreased the maximum principal strain with the cost of decrease in normalized (norm.) mass and increase in recoil. For each material, the applicable results of the optimized designs were similar. Since the stents with a shorter unit length can provide better scaffolding,²⁹ such optimized designs were chosen for the 3D model (M_{3d}) testing, as underlined in Table 2.

2D Validation Testing Results

In the recoil experimental testing, a total displacement of 20.9 mm was imposed between the bases of the AZ31 specimens (Fig. 9a). The original and optimized designs had an average recoil ratio of 7.8% and 8.5%, respectively; the optimized designs increased the recoil, which is in agreement with the numerical results. Regarding the tensile rupture tests, the original design broke at the displacement of 40 mm, while the optimized design at the displacement of 47 mm, showing that the optimized design was safer than the original

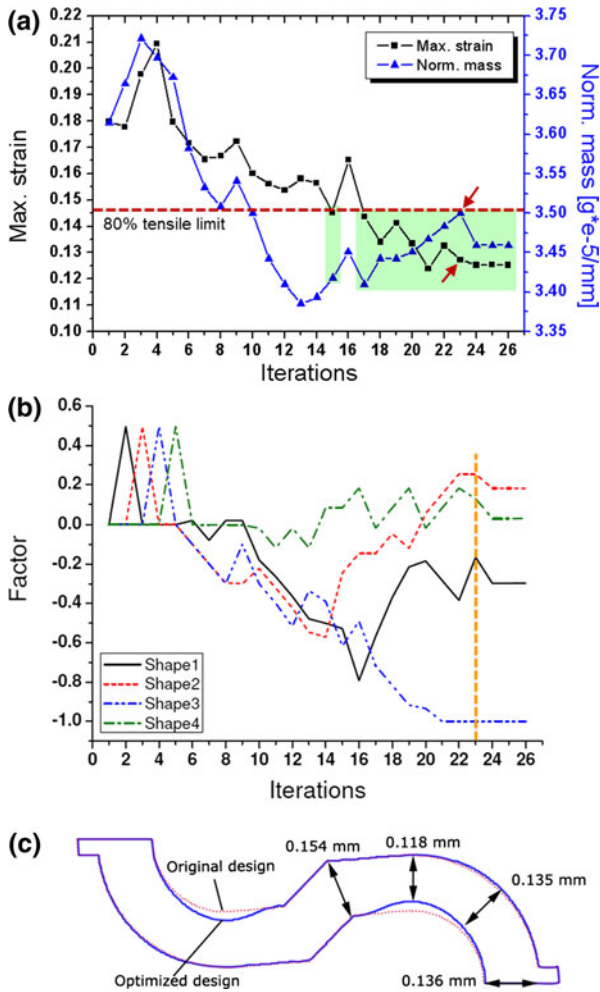


FIGURE 7. Optimization results of the WE43 M_{2d} with unit length of 1.22 mm: (a) Optimization history of responses of maximum (max.) principle strain and normalized (norm.) mass. The results with the maximum principle strain below Opt-limit (80% tensile limit) were shaded for distinction. The M_{2d} of iteration 23 (indicted by arrows) was chosen as the optimized design. (b) Optimization history of shape variations. Iteration 23 was indicated with the vertical dotted line. (c) Layout comparison of the original design and the optimized design (after being projected to the 2D outer surface). The main dimensions of the optimized design were indicated. The narrowest width is 0.118 mm in the straight parts of the strut.

one during expansion (Fig. 9b). The break location of the original design was compatible to the stress concentrated area in the simulation (Fig. 8a).

3D Results

The 3D stent models of AZ80 and AZ31 had a total length of 8.13 mm, while the models of ZM21 and WE43 of 7.43 mm. The testing procedure of the WE43 M_{3d} showed a typical “dog-bone” phenomenon during stent expansion (Fig. 10). When the balloon was fully inflated, the stent reached the outer diameter of 3.05 mm. When the balloon was retrieved, the stent recoiled with the tissue and reached the final diameter of 2.83 mm.

The WE43 M_{3d} had the lowest recoil, the lowest maximum principal stress after recoil and the second highest normalized mass of the four optimized models (Table 3); therefore, it was chosen as the final optimized design (FOD). Although both the FOD and the Magic stent had the same constitutive material model, the FOD decreased the recoil, the maximum principal strain, and the maximum principle stress after recoil by 24, 14, and 29%, respectively. Furthermore, the FOD increased the normalized mass by 58%, and the narrowest strut width was 0.118 mm. Figure 11 shows the comparison between the Magic stent and the FOD on the distribution of maximum principal strain and stress. The Magic stent had local concentrations of both strain and stress, whereas the FOD had a more even distribution of strain and stress, well compatible with the results of the M_{2d} .

DISCUSSION

The *in vivo* degradation of MAS consists of both uniform and stress corrosion, influenced by the strut width/mass and the maximum principle stress/strain, respectively. The final optimized design increased the strut width by 48% at least compared to the existing

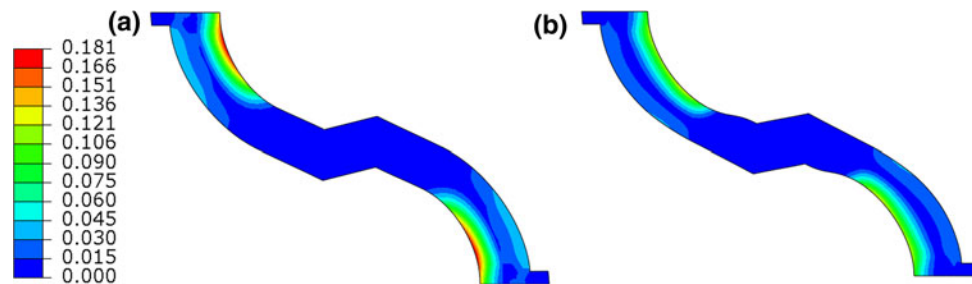


FIGURE 8. Strain distribution of the WE43 M_{2d} with a unit length of 1.22 mm: (a) original design and (b) optimized design.

TABLE 2. Result summary of 2D shape optimization.

Design	Unit length of 1.45 mm			Unit length of 1.36 mm			Unit length of 1.22 mm			
	Max. strain	Norm. mass (g*e-5/mm)	Recoil (%)	Max. strain	Norm. mass (g*e-5/mm)	Recoil (%)	Max. strain	Norm. mass (g*e-5/mm)	Recoil (%)	
AZ80	Original	0.129	3.56	9.8	0.148 ^a	N.A.	N.A.	0.190 ^a	N.A.	N.A.
	Optimized	0.104	3.48	10.5	<u>0.103</u>	<u>3.40</u>	<u>10.0</u>	0.122 ^b	N.A.	N.A.
AZ31	Original	0.126	3.56	7.3	0.145	3.58	6.4	0.187 ^a	N.A.	N.A.
	Optimized	0.116	3.51	7.5	<u>0.112</u>	<u>3.46</u>	<u>7.0</u>	0.123 ^b	N.A.	N.A.
ZM21	Original	0.132	3.56	7.0	0.154	3.58	6.1	0.201 ^a	N.A.	N.A.
	Optimized	-	-	-	0.134	3.50	6.5	<u>0.127</u>	<u>3.51</u>	<u>5.7</u>
WE43	Original	0.133	3.56	5.2	0.149	3.58	4.5	0.180	3.61	3.4
	Optimized	-	-	-	0.142	3.52	4.6	<u>0.127</u>	<u>3.50</u>	<u>4.0</u>

-: optimization was not needed; ^a the maximum strain of original design was beyond tensile limit; ^b the maximum strain of optimized design was beyond Opt-limit.

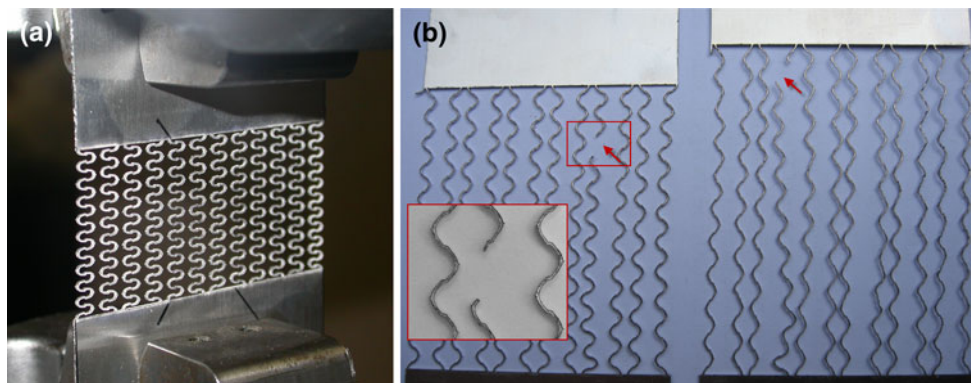


FIGURE 9. (a) A laser-cut AZ31 specimen of the optimized design during the recoil testing. It has 12 rings composed by 10 struts (20 units) each, being available a cutting area of 50 mm × 16.35 mm. (b) Comparison of the two AZ31 samples with original design (left) and optimized design (right) after fracture test. The optimized design ruptured at higher elongation.

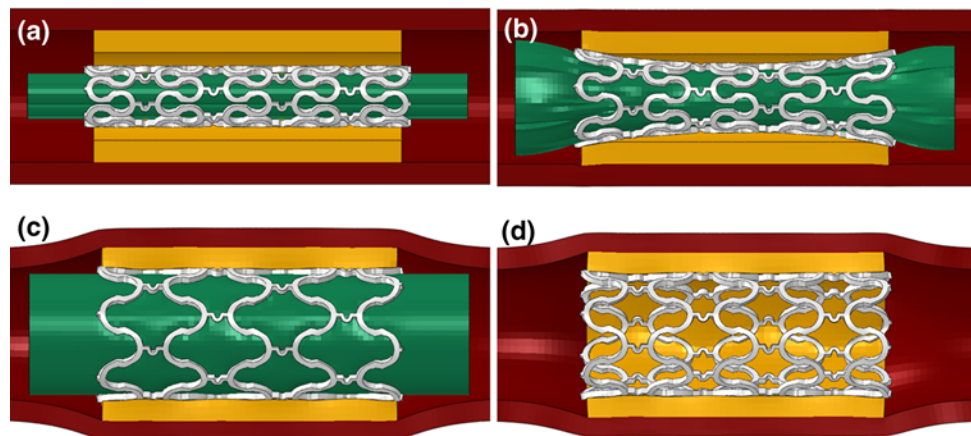


FIGURE 10. The 3D simulation of stent expansion inside the arterial vessel for the WE43 M_{3d} with a unit length of 1.22 mm: (a) before balloon expansion; (b) during balloon expansion; (c) full balloon expansion; and (d) the balloon was retrieved and the stent recoiled together the arterial tissues.

MAS. Accordingly, the FOD is expected to extend the degradation time with the same uniform corrosion rate. The maximum principal stress is critical for MAS

because high stress can accelerate stress corrosion. The decrease of the maximum principle stress after recoil (29%) and the more uniform stress distribution of

TABLE 3. Result summary of 3D model testing.

		Max. principle strain	Norm. mass (g*e-4/mm)	Recoil with vessel (%)	Max. principle stress after recoil (MPa)
Magic	WE43	0.153	2.37	8.2	230
	AZ80	0.103	3.69	11.8	230
Optimized design	AZ31	0.105	3.74	9.2	196
	ZM21	0.127	3.76	7.2	188
	WE43	0.132	3.75	6.2	163

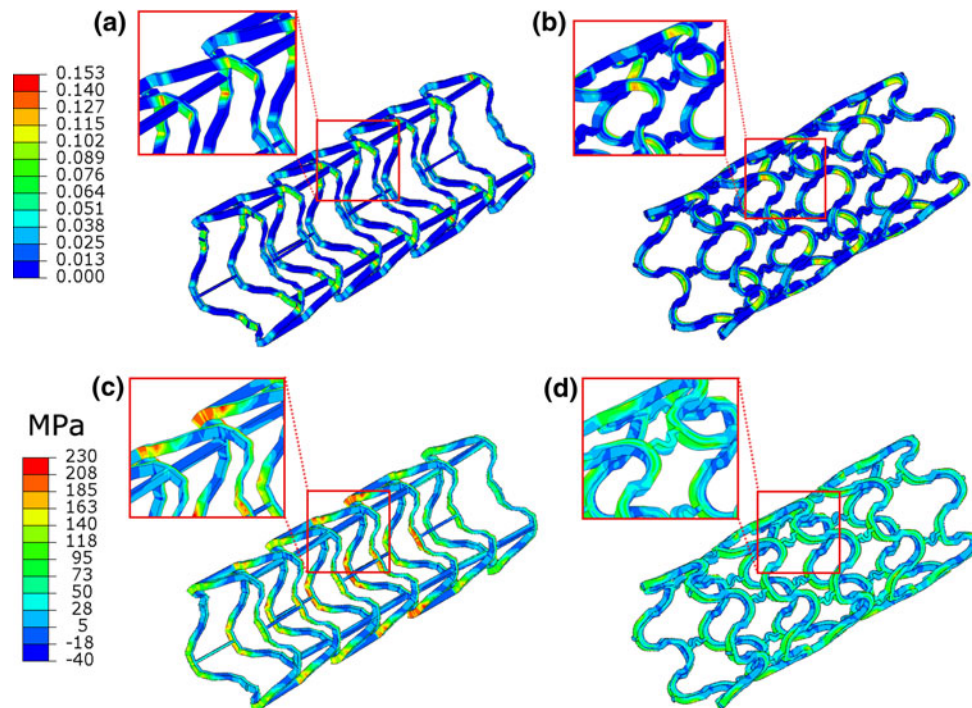


FIGURE 11. Comparison of the maximum principle strain between (a) the Magic stent and (b) the M_{3d} of WE43. Comparison of the maximum principle stress after stent recoil between (c) the Magic stent and (d) the M_{3d} of WE43.

FOD should result in slower stress corrosion.²⁸ It should be noted that although an increased strut width could extend the uniform corrosion time, a wider strut may increase the maximum principle stress during stent expansion and after recoil, which could lead to accelerated stress corrosion. Since the integrity of a MAS is usually broken first in the stress-concentrated locations,²² it can be estimated that stress corrosion should play a major role in the failure of a MAS. Therefore, reducing maximum principle stress/strain should be the priority in optimization to maintain structural integrity. In addition, FOD improved the structural safety during stent expansion and the scaffolding properties by decreasing the maximum principal strain and recoil, respectively. To the author's knowledge, this is the first study on stent design optimization with magnesium alloys.

During optimization, the morphing procedure was applied on the model mesh directly and the shape variations were also based on changes of the original mesh. It implies that once the mesh of the optimization model (M_{2d}) is created and the shape variations are set, all the shape changes derive from only one original mesh. As for the conventional shape optimization in which the shape changes are based on geometry files, each new design needs a new meshing procedure and this may cause lots of repeated works, especially for complicated shapes which cannot be meshed automatically.^{11,23} Furthermore, although different software tools were involved in optimization, optimization strategy adopted here transformed data and evolved optimization automatically. The optimization evolution was convenient without any manual interaction.

As pointed out by previous works,^{4,14} the 2D model can effectively represent the corresponding 3D solid model (Figs. 8 and 10), though the 3D model has curved structure and contact behaviors. There are three benefits of the 2D model: (i) it can greatly simplify the setting of shape variations compared to the 3D model, because the 3D model must consider the influence of the structural curvature on the shape changes; (ii) the 2D model can significantly reduce the cost in simulation time: on the same hardware, one iteration of 2D model costs seconds while the 3D model several minutes; (iii) there is minimal convergence failure in the 2D model.

The strut width is usually constant in conventional stent designs,¹ like in the Magic stent. However, the strut width of FOD is not uniform (Fig. 7c): the mass at the inner straight parts was reduced more and the mass at the outer curved parts was added, which decreased the maximum strain and produced a more uniform strain distribution (Fig. 8). This implies that changes of the mass distribution along the strut may be a useful method to optimize the stent property, especially for stents of low ductility materials. On the other hand, increased strut width also influences stent flexibility and arterial damages. Stent flexibility is mainly controlled by the shape and location of stent links.^{14,19} To avoid the adverse influence of increased width on stent flexibility, the links of the FOD have a smaller width (0.08 mm) than the struts (0.14 mm); moreover, a “U” shape design is applied to increase flexibility. Arterial damages are influenced by high arterial stresses during stent scaffolding.¹⁰ To scaffold the same artery, the wider strut can provide more contact area and consequently could decrease arterial stress. Furthermore, it should be noted that the structural modification of optimized design is finely detailed, which may not survive the conventional manufacturing and electropolishing methods. Femtosecond laser cutting is recommended for manufacturing, which can provide high accuracy and be followed by very little electropolishing.²⁰

Strut thickness of the FOD is same as the Magic because increasing thickness could increase disruptive effects on blood flow and thrombogenesis potential.⁸ Most metal stents are currently manufactured from uniform tubes and have uniform thickness, thus the optimization was carried out on a 2D section of the stent strut, with an assumed constant thickness. However, a non-uniform stent thickness may lead to further enhancement of the design, which can provide more shape parameters in an optimization. A non-uniform thickness design may be realized with the development of stent manufacture methods.

It can be observed from Tables 1 and 3 that material properties, especially the ultimate elongation, affect

optimization results greatly. Increasing ductility of magnesium alloys is an important way to improve mechanical properties of MAS. Moreover, although ZM21 and WE43 have the same ultimate elongation, the final results of the two materials were different, as shown in Table 3. It implies that an optimization result is specific to the material and that the testing of material property should be accurate to get reliable optimization results.

Two criterions were set for the optimization: the Opt-limit controlled the applicable results chosen for the optimized design and, the range of shape variations controlled the possible dimension ranges applied in optimization. The two criterions can provide flexible controls on the optimized design for different design demands. For example, if the material is more brittle, the Opt-limit should be decreased for a safe design.

When unit length decreases, the maximum principal strain (both in the original and optimized designs) may be beyond the ultimate elongation. It is interesting to observe that even if the maximum principal strain of the original design is beyond the ultimate elongation, that of optimized design can still be below the Opt-limit (i.e., AZ80 M_{2d} with the unit length of 1.36 mm). It can be estimated that there is a unit length limit where the maximum principal strain cannot be optimized to be below Opt-limit. This could be another way to define the unit length and more work should be done in the future to test the reliability.

One limitation of this study is that the mechanical properties of WE43 were deduced from the literature and the stress–strain tensile curve was not as “realistic” as the other materials. However, this study is focused on the methodology of optimization and the FOD model used the same material when comparing it to the existing stent. Another limitation is that the processes of stent crimping, deployment (tracking through tortuous vessels), and degradation were not modeled. For example, the applied maximum principle stress was from expansion and recoil; however, crimping and deployment can apply additional stress to the model and the stress should continue changing during degradation. A more realistic model that considers crimping and deployment should be built into future works. In addition, although the degradation process is not directly considered in the optimization strategy, the resulting FOD could be considered a suitable compromise thanks to the increase of the material and the more uniform distribution of stresses.

CONCLUSIONS

A new MAS design was shape-optimized using a 2D model of a repeating stent unit. The change of mass

distribution along the strut can be a useful way to reduce strain and stress concentration during stent expansion and scaffolding. A morphing procedure greatly facilitated setting of new model shapes. The optimization was carried out by automatic evolution. Two experiments were carried out for a preliminary validation of the 2D models with good results. The final optimized 3D design increased the strut width by 48% at least, decreased the maximum principal strain by 14%, decreased maximum principle stress after recoil by 29%, and enhanced scaffolding ability by 24%, compared to the existing MAS design with the same material WE43. Accordingly, it is expected that the corrosion behavior is improved in the optimized model. The method provides a convenient and practical way to optimize properties of novel MAS designs.

ACKNOWLEDGMENTS

The research is supported by a grant from the Fondazione Cassa di Risparmio di Trento e Rovereto, the financial support of the IIT through the project 'Models and Methods for Degradable Materials' and the financial support of the Politecnico di Milano through the project 'Development of bioabsorbable magnesium alloy innovative stents'.

REFERENCES

- ¹Capelli, C., F. Gervaso, L. Petrini, G. Dubini, and F. Migliavacca. Assessment of tissue prolapse after balloon-expandable stenting: influence of stent cell geometry. *Med. Eng. Phys.* 31:441–447, 2009.
- ²Dalla Torre, F. H., A. C. Hanzi, and P. J. Uggowitzer. Microstructure and mechanical properties of microalloyed and equal channel angular extruded Mg alloys. *Scripta Mater.* 59:207–210, 2008.
- ³De Beule, M., P. Mortier, S. G. Carlier, B. Verheghe, R. Van Impe, and P. Verdonck. Realistic finite element-based stent design: the impact of balloon folding. *J. Biomech.* 41:383–389, 2008.
- ⁴Donnelly, E. W., M. S. Bruzzi, T. Connolley, and P. E. McHugh. Finite element comparison of performance related characteristics of balloon expandable stents. *Comput. Methods Biomech. Biomed. Eng.* 10:103–110, 2007.
- ⁵Erbel, R., C. Di Mario, J. Bartunek, J. Bonnier, B. de Bruyne, F. R. Eberli, P. Erne, M. Haude, B. Heublein, M. Horrigan, C. Ilesley, D. Bose, J. Koolen, T. F. Luscher, N. Weissman, R. Waksman, and P.-A. Investigators. Temporary scaffolding of coronary arteries with bioabsorbable magnesium stents: a prospective, non-randomised multicentre trial. *Lancet* 369:1869–1875, 2007.
- ⁶Gervaso, F., C. Capelli, L. Petrini, S. Lattanzio, L. Di Virgilio, and F. Migliavacca. On the effects of different strategies in modelling balloon-expandable stenting by means of finite element method. *J. Biomech.* 41:1206–1212, 2008.
- ⁷Gu, X. N., Y. F. Zheng, Y. Cheng, S. P. Zhong, and T. F. Xi. In vitro corrosion and biocompatibility of binary magnesium alloys. *Biomaterials* 30:484–498, 2009.
- ⁸Kastrati, A., J. Mehilli, J. Dirschinger, F. Dotzer, H. Schühlen, F. J. Neumann, M. Fleckenstein, C. Pfafferoth, M. Seyfarth, and A. Schömig. Intracoronary stenting and angiographic results: strut thickness effect on restenosis outcome (ISAR-STERO) trial. *Circulation* 103:2816–2821, 2001.
- ⁹Kiousis, D., A. Wulff, and G. Holzapfel. Experimental studies and numerical analysis of the inflation and interaction of vascular balloon catheter-stent systems. *Ann. Biomed. Eng.* 37:315–330, 2009.
- ¹⁰Lally, C., F. Dolan, and P. J. Prendergast. Cardiovascular stent design and vessel stresses: a finite element analysis. *J. Biomech.* 38:1574–1581, 2005.
- ¹¹Li, N., H. W. Zhang, and H. J. Ouyang. Shape optimization of coronary artery stent based on a parametric model. *Finite Elem. Anal. Des.* 45:468–475, 2009.
- ¹²Marry, V. R., R. Burgermeister, R. B. Grishaber, and R. O. Ritchie. Fatigue and life prediction for cobalt-chromium stents: a fracture mechanics analysis. *Biomaterials* 27:1988–2000, 2006.
- ¹³McGarry, J. P., B. P. O'Donnell, P. E. McHugh, and J. G. McGarry. Analysis of the mechanical performance of a cardiovascular stent design based on micromechanical modelling. *Comp. Mater. Sci.* 31:421–438, 2004.
- ¹⁴Mori, K., and T. Saito. Effects of stent structure on stent flexibility measurements. *Ann. Biomed. Eng.* 33:733–742, 2005.
- ¹⁵Muller, H. Development of metallic bioabsorbable intravascular implants. In: *New Technologies in Vascular Biomaterials. Connecting Biomaterials to Arterial Structures*, edited by N. Chakfé, and B. Durand. Strasbourg: Europrot, 2009, pp. 23–32.
- ¹⁶Peeters, P., M. Bosiers, J. Verbist, K. Deloose, and B. Heublein. Preliminary results after application of absorbable metal stents in patients with critical limb ischemia. *J. Endovasc. Ther.* 12:1–5, 2005.
- ¹⁷Pelton, A. R., V. Schroeder, M. R. Mitchell, X. Y. Gong, M. Barney, and S. W. Robertson. Fatigue and durability of Nitinol stents. *J. Mech. Behav. Biomed. Mater.* 1:153–164, 2008.
- ¹⁸Pericevic, I., C. Lally, D. Toner, and D. J. Kelly. The influence of plaque composition on underlying arterial wall stress during stent expansion: the case for lesion-specific stents. *Med. Eng. Phys.* 31:428–433, 2009.
- ¹⁹Petrini, L., F. Migliavacca, F. Auricchio, and G. Dubini. Numerical investigation of the intravascular coronary stent flexibility. *J. Biomech.* 37:495–501, 2004.
- ²⁰Rizvi, N. H. Femtosecond laser micromachining: current status and applications. *RIKEN Rev.* 50:107–112, 2003.
- ²¹Schranz, D., P. Zartner, I. Michel-Behnke, and H. Akinturk. Bioabsorbable metal stents for percutaneous treatment of critical reoarterctation of the aorta in a newborn. *Catheter. Cardio. Inte.* 67:671–673, 2006.
- ²²Slottow, T. L. P., R. Pakala, and R. Waksman. Serial imaging and histology illustrating the degradation of a bioabsorbable magnesium stent in a porcine coronary artery. *Eur. Heart J.* 29:314, 2008.
- ²³Timmins, L. H., M. R. Moreno, C. A. Meyer, J. C. Criscione, A. Rachev, and J. E. Moore. Stented artery

- biomechanics and device design optimization. *Med. Biol. Eng. Comput.* 45:505–513, 2007.
- ²⁴Tsimikas, S. Drug-eluting stents and late adverse clinical outcomes—lessons learned, lessons awaited. *J. Am. Coll. Cardiol.* 47:2112–2115, 2006.
- ²⁵Waksman, R. Promise and challenges of bioabsorbable stents. *Catheter. Cardio. Inte.* 70:407–414, 2007.
- ²⁶Waksman, R., R. Pakala, P. K. Kuchulakanti, R. Baffour, D. Hellinga, R. Seabron, F. O. Tio, E. Wittchow, S. Hartwig, C. Harder, R. Rohde, B. Heublein, A. Andreae, K. H. Waldmann, and A. Haverich. Safety and efficacy of bioabsorbable magnesium alloy stents in porcine coronary arteries. *Catheter. Cardio. Inte.* 68:607–617, 2006.
- ²⁷Wang, G. G., Z. M. Dong, and P. Aitchison. Adaptive response surface method—a global optimization scheme for approximation-based design problems. *Eng. Optimiz.* 33:707–733, 2001.
- ²⁸Winzer, N., A. Atrens, W. Dietzel, G. Song, and K. U. Kainer. Stress corrosion cracking in magnesium alloys: characterization and prevention. *JOM* 59:49–53, 2007.
- ²⁹Wu, W., M. Qi, X. P. Liu, D. Z. Yang, and W. Q. Wang. Delivery and release of nitinol stent in carotid artery and their interactions: a finite element analysis. *J. Biomech.* 40:3034–3040, 2007.
- ³⁰Wu, W., D. Z. Yang, Y. Y. Huang, M. Qi, and W. Q. Wang. Topology optimization of a novel stent platform with drug reservoirs. *Med. Eng. Phys.* 30:1177–1185, 2008.